Rotating Rayleigh-Bénard Convection: Aspect Ratio Dependence of the Initial Bifurcations

Li Ning and Robert E. Ecke

Physics Division and Center for Nonlinear Studies

Los Alamos National Laboratory, Los Alamos, NM 87545

February 9, 2008

Abstract

The initial bifurcations in rotating Rayleigh-Bénard convection are studied in the range of dimensionless rotation rate $0 < \Omega < 2150$ for an aspect-ratio-2.5 cylindrical cell. We used simultaneous optical shadowgraph, heat transport and local temperature measurements to determine the stability and characteristics of the azimuthally-periodic wall convection state. We also show that the second transition corresponds to the onset of bulk convection. Our results for critical Rayleigh numbers, precession frequencies and critical mode numbers agree well with theoretical results. The dynamics of the wall convection state can be described by a complex Ginzburg-Landau amplitude equation.

1 Introduction

Studying the effects of external rotation on thermal convection has attracted significant experimental and theoretical interest [1, 2, 3, 4]. Because of its general occurrence in geophysical and oceanic flows, it is important to understand how the Coriolis force influences the structure and transport properties of thermal convection. Rotating thermal convection also provides a system in which to study hydrodynamic instabilities [3, 5, 6], pattern formation and spatio-temporal chaos in nonlinear dynamical systems [4, 7], and transitions to turbulence [8, 9].

Rayleigh-Bénard convection consists of a fluid layer confined between two horizontal plates and heated from below. External rotation is imposed by rotating the convection cell about a vertical axis. Most theoretical studies of this system have assumed a laterally infinite cell geometry [1]. In experiments, however, there are always side walls. Moreover, to achieve sufficient laboratory control over the experimental parameters and obtain large dimensionless rotation rates, the horizontal dimensions of the convection cells are usually comparable to their vertical depths. This raises the question whether the theoretical predictions for infinitely extended systems are relevant for real experiments. It has indeed been found that the presence of lateral boundaries change significantly some aspects of thermal convection in the presence of rotation[3, 4, 6]. In this paper, we present experimental results that illustrate clearly the influence of the lateral boundaries. We confine ourselves to cylindrical convection cells and characterize the geometry by the aspect ratio which is the ratio of the radius to the depth.

There have been several experimental and theoretical investigations on rotating Rayleigh-Bénard convection. One of the early quantitative experiments by Rossby[3] showed significant deviation from the predictions of theories for a laterally infinite system. His measurement of heat transport showed a slow increase over the pure conduction state at temperature differences much smaller than the expected onset of convection for an infinitely extended system. There have been many explanations offered to remedy this discrepancy. The first one that correctly attributed the increase in thermal transport to a side wall convection state was proposed by Buell and Catton[6]. They investigated the stability of the conduction state in a laterally finite cylinder in the presence of rotation. Contrary to conventional wisdom that side walls suppress thermal convection, they found that for a large enough rotation rate, some side wall convection states have a critical control parameter that is much lower than the value for the laterally infinite case. These non-axisymmetric wall states are azimuthally periodic and have maximum amplitude near the side wall. Zhong *et al*[4] later reported experimental confirmation of the wall convection states in a unit aspect ratio cell. They observed, however, that these asymmetric states precessed slowly counter to the direction of rotation. In addition to the first bifurcation to the wall states, there was a second bifurcation when the central region became filled with vortex-like structures, accompanied by an increase in the thermal transport and in the thermal noise measured in the bottom plate.

Goldstein *et al*[10] carried out a linear stability analysis which allowed for the experimentally observed precession and found good agreement with the experimental results. Ecke *et al*[11] explained the traveling wall states by a broken azimuthal reflection symmetry and predicted that the precession frequency would go linearly to zero as the rotation rate went to zero[11].

Our experiment, using an aspect ratio 2.5 cell, was designed to explore the aspect ratio dependence of the initial bifurcation from the conduction state to the wall convection state. We chose to increase the aspect ratio only moderately relative to the previous cell of Zhong et al [4] because the range of accessible dimensionless rotation rates (limited by the condition that centrifugal effects be small) for the larger aspect ratio cell overlapped a large fraction of the parameter range used in the previous work. Furthermore, although the physical aspect ratio is considered small for nonrotating convection, rotation increases the effective aspect ratio significantly. In addition, since the side-wall state forms around the azimuth, the number of structures that fit in that geometry is roughly the ratio of the perimeter to twice the depth. For $\Gamma = 2.5$ this ratio is 7.9. Thus, provided the dimensionless rotation rate is sufficiently large, one can consider the conditions to be in the moderate to large aspect ratio limit and our measurements presented here together with the previous work for $\Gamma = 1$ suffice to characterize the aspect ratio dependence of the observed bifurcations. We discuss this in more detail later.

In this work we present measurements of the critical Rayleigh numbers and critical wavenumbers for the initial transition to a side-wall traveling wave state and the second transition to bulk convection. We find that the traveling wave state can be described quantitatively by a one-dimensional complex Ginzburg-Landau (CGL) equation. In addition we find that the traveling wave state does not depend on the overall geometry of the convection cell. Rather it exists on any wall regardless of the magnitude or sign of the wall curvature. Further, the conductivity of the wall is shown to strongly influence the critical Rayleigh number for the bifurcation to traveling waves. Finally, the second transition to bulk convection is shown to occur as a spatially seperate transition owing to the negligible amplitude of the wall state in the center of the cell.

2 Experiment

The apparatus used in these convection studies was descibed in detail by Zhong *et al*[4]. The bottom plate of the convection cell was a nickel-plated, mirror-polished, copper plate with a thermofoil heater attached to the back. The top plate was a 1/8 *inch* thick, optical quality sapphire window. The side wall was made of 0.31 cm thick plexiglasss, defining an active circular area with a radius $r = 5.00\ cm$. The depth d of the cell was 2.00 cm, giving an aspect ratio $\Gamma = r/d = 2.5$. We used an afocal optical shadowgraph technique to visualize the convective flow field. Because of the depth of the cell (hence a very small temperature gradient), the shadowgraph method was not sensitive enough to observe the flow near the first bifurcation, especially when the rotation rate was small. For local temperature measurement, two thermistors were embedded at half-height positions in the side wall with known angular separation. Since the wall states traveled along the circumference, the thermistors measured the temperature field sweeping by. From these data, the amplitude, frequency and mode number of the traveling wave were extracted. The heating was provided by applying a constant voltage to the bottom heater, and a circulating, temperature-regulated water bath outside the top sapphire window provided cooling and constant top temperature to better than 0.5 mK rms. Since the convection cell rotates relative to the regulated water bath, the top-plate temperature is azimuthally very uniform on the time scale relevant to the dynamics of the system. Thermistors embedded in the bottom plate and near the top plate measured the respective temperatures to a precision better than 0.1 mK. Rotation was provided with a stepper motor with rotation frequency constant to $\pm 0.1\%$. Because the shadowgraph optics was at rest in the laboratory, a shaft encoder strobed the video camera at each revolution of the cell. The image digitized via a digital frame grabber was thus synchronized with the rotating cell. Since the dynamics of the convection patterns were slow compared to the rotation period, we did not lose any detailed information by recording the images once per revolution.

The control parameters of the experiment are Rayleigh number R and dimensionless rotation rate Ω, defined as $R = \alpha g d^3 \Delta T/\kappa\nu$ and $\Omega = \Omega_D d^2/\nu$, where α, κ and ν are the thermal expansion coefficient, thermal diffusivity and kinematic viscosity of the working fluid, g is the gravitational acceleration, ΔT is the bottom-top temperature difference and Ω_D is the angular

rotation frequency. Another parameter that characterizes the fluid is the Prandtl number $P = \nu/\kappa$, which is about 6.4 for our choice of water at a mean temperature of about $23.5°C$. A reduced bifurcation parameter is defined as $\epsilon = (R - R_c(\Omega))/R_c(\Omega)$, where $R_c(\Omega)$ is the critical Rayleigh number for the onset of the first convection state at a particular Ω. As we will dicuss below, the first bifurcation can be to different states depending on Ω. Therefore, we denote the critical Rayleigh number for the side-wall state as R_{cs} and that for the onset of bulk convection as R_{cb}. The effect of the centrifugal force can be characterized by the ratio of the centrifugal-to-gravitational force, $\Omega_D^2 r/g$, which is less than 0.12 for our maximum rotation rate $\Omega_D \approx 4.9$ rad/sec ($\Omega \approx 2145$).

The experimental protocol we used was as follows: Ω_D was held constant for the desired Ω at ΔT_c; the heating was quasistatically ramped to each measurement point. After several vertical thermal diffusion times $\tau_\kappa = d^2/\kappa \approx 2760$ *sec*, measurement of temperatures were made spanning at least one τ_κ. Shadowgraph images were recorded at fixed time intervals during the temperature measurements. We followed the dynamics at several parameter values for longer than $40\tau_\kappa$, and no change of the convection states was found for the parameter range studied. There is one exception concerning the stability of the wall state which will be discussed later.

For determining the onset of the wall convection state, two different measurements were used for large enough values of Ω so that the transition to the wall state was the first bifurcation. For smaller Ω only the second method was used. The first was the measurement of heat transport, expressed in Nusselt number Nu which is the ratio of the heat transported by the convection state to the heat transported by conduction alone. In the conduction state $Nu = 1$ whereas just above the onset of convection, Nu increases linearly with increasing R. The intercept of the linear section of Nu versus R with $Nu = 1$ determines R_{cs}. The second method used the temperature measurements from the side wall thermistors T_{md1} and T_{md2}. By fitting the oscillatory signals to a sine function, we extracted the amplitude δT, which rises above the onset of the side wall state as $(R - R_{cs}(\Omega))^{1/2}$. The two methods yielded values of R_c that agreed to within experimental uncertainty, usually better than 0.2%. The second method also gave us the frequency and mode number of the traveling wave.

The second bifurcation was determined by the Nusselt number measurement. We did, however, find two other characteristics of the bulk convection

state that could be used to determine the onset, namely, the thermal noise in the bottom temperature and the amplitude of the shadowgraph images. These results will be discussed in detail later.

3 Experimental Results and Comparison with Theories

We present our experimental results on an aspect ratio 2.5 cell. When appropriate for showing variation as a function of aspect ratio, we also include results for the unit aspect ratio cell from Zhong *et al*[4]. Comparison with theories are made whenever theoretical results are available.

3.1 Asymmetric wall convection states

As the temperature difference between the bottom and top plates increases at fixed Ω (Ω actually changes slightly in the experiment since we held Ω_D constant; typically, Ω varies less than 0.4% for the range of Rayleigh numbers we used), the first bifurcation from the quiescent conduction state is to an azimuthally periodic wall convection state for moderate to high rotation rates. This convection state precesses uniformly in the rotating frame, counter to the direction of external rotation and with maximum amplitude near the side wall. The amplitude grows above the onset as $\epsilon^{1/2}$ and the frequency ω_κ changes linearly with ϵ and has a finite value at onset. This indicates that the bifurcation is a forward Hopf bifurcation. The unique direction of precession arises from the weak breaking of azimuthal reflection symmetry by the external rotation (Ecke *et al*)[11]. The ϵ dependence of the amplitude and the frequency of the wall convection state is adequately characterized in Zhong *et al*[4]. We concentrate on the Ω dependence of the critical frequencies and mode numbers, and in particular, on their behaviors as Ω goes to zero or becomes large. We also discuss the linear stabilities for different mode-number wall convection states.

We have measured the critical Rayleigh number of the wall convection states in a wide range of Ω. The results are displayed in Figure 1. The dashed line is from the calculations of Goldstein *et al* for perfectly insulating side walls[10], corresponding reasonably well with the experimental boundary conditions (plexiglass side wall). The agreement between experiments and

Figure 1: Parameter-space diagram of rotating Rayleigh-Bénard convection in small aspect ratio cylindrical containers. Measured bifurcation points from conduction to wall convection ($\triangle$) and bulk convection states ($\triangle$) for an aspect ratio 2.5 cell and corresponding bifurcation points ($\bullet$ and $\circ$) measured in a unit aspect ratio cell[4] are shown. Rossby's results (+) for aspect ratios 1.4-5[3], Chandrasekhar's linear stability calculation for a laterally infinite system (—), and Goldstein *et al*'s result (- - - -) for a unit aspect ratio cell with insulating side walls[10] are also shown for comparison.

theory is very satisfactory. The results of Zhong *et al* for $\Gamma = 1$ are also shown in Figure 1. For completeness, we have included experimental data of Rossby[3] using cylindrical convection cells with a range of aspect ratios from 1.4 to 5.0. There is not much variation in R_{cs} among these cell geometries for $\Omega > 100$. We believe that the wall-state bifurcation curve is quite insensitive to further increases in Γ. The other bifurcation line and the cross-over of the two bifurcation lines in $\{R, \Omega\}$ parameter space will be discussed later.

Figure 2 shows the measured precession frequency at onset $\omega_{\kappa 0}$ scaled by τ_κ for the wall states versus Ω in a semi-log plot. The inset shows the linear dependence of the critical frequency on Ω for $\Omega < 150$. The large Ω behavior of $\omega_{\kappa 0}$ suggests a nearly logarithmic dependence on Ω. Notice that for high Ωs, the frequencies for aspect ratios 1 and 2.5 cells approach each other.

Figure 2: Comparison of experimental and theoretical results on the precession frequencies of the wall convection states. Data for aspect ratio 2.5 (∘) and 1 (•) cells, Goldstein *et al*'s results (—) for a unit aspect ratio cell, and the results of Kuo and Cross (-·--·-) for a planar wall state. The inset is a linear plot of the frequencies at small rotation rate and the dashed line is a fit to the data.

Ω	R_{cs} 10^4	$\omega_{\kappa 0}$	m_c	λ_c	R_{cb} 10^4	k_{cb}
0	—	—	—	—	0.18	—
16.93	0.33	1.98	6	2.62	0.24	—
33.86	0.38	5.0	8	1.96	0.35	—
67.70	0.64	9.1	10	1.57	0.69	—
135.5	1.14	16.7	10	1.57	1.5	7.0
271.0	2.16	22.8	11	1.43	3.4	7.9
545.8	4.51	30.25	12	1.31	8.13	11.3
1091	9.15	35.2	12	1.31	21.5	13.9
2145	18.1	38.5	13	1.21	52.2	18.5

Table 1: Values of Ω, R_{cs}, $\omega_{\kappa 0}$, m_c, λ_c, R_{cb}, and k_{cb}.

The solid line in the figure comes from a recent calculation by Goldstein *et al* for a unit aspect ratio geometry[10]. Their calculation also shows that for moderately high Ω, the change in frequency with increasing aspect ratio is small for $\Gamma > 1$. The dash-dotted curve is the result for infinite aspect ratio cells with insulating rigid side wall and free-free top-bottom boundary conditions from Kuo and Cross[12].

The critical mode numbers m_c of the wall states were measured by quasistatically increasing ΔT from below. To scale out the aspect ratio dependence and identify the trend as both Γ and Ω increase, we convert the mode numbers to dimensionless azimuthal wavelengths scaled by the depth d, so that $\lambda_c = 2\pi\Gamma/m_c$. In Table 1 we show data for the onset of the side-wall state denoted R_{cs}, $\omega_{\kappa 0}$, m_c, λ_c, and the critical Rayleigh number R_{cb} and the critical wavenumber k_{cb} for bulk convection for the full range of Ω values we explored for the Γ=2.5 convection cell. Figure 3 shows λ_c versus Ω for Γ of 1 and 2.5. The numbers in parentheseses near the data points are the corresponding mode numbers. The stepped solid line is from Goldstein *et al*[10] for $\Gamma = 1$. The large Ω behavior of λ_c suggests that it approaches a value near 1 or, in other words, that the critical mode number approaches a finite constant. This implies that the depth of the convection cell is setting the spatial scale of this wall state.

We can understand the behavior of $m_c(\Omega)$ in the following manner: using

Figure 3: The critical wavelength for wall convection states with Γ=2.5 ($\circ$) and Γ=1 ($\bullet$). The bracketed numbers are the corresponding mode numbers. The solid line is from Goldstein *et al* for a unit aspect ratio cell and the dash-dotted curve is from Kuo and Cross for a planar wall state.

a physical argument by Manneville[13], we know that to minimize the dissipation losses due to vertical and horizontal shear, the convection rolls should have similar width and height. In the case of wall convection in the presence of rotation, since 1) the Coriolis force only serves to skew the particle trajectories without providing kinetic energy, and 2) there is additional viscous damping in the vertical direction because the wall states lie close to the side wall, the convection structure should have a width comparable to but narrower than if it was not near a rigid wall. This leads to a critical wavelength in the streamline plane less than 2 for the wall states. In the bulk convection, external rotation gives rise to increasing apparent wavenumbers(measured as the distance between the periodic structures) as Ω increases[14]. In our experiment, since the particle trajectories near the side wall have to be nearly parallel to the wall, the measured wavelength is in the streamline plane. From the radial basis functions for the velocity and temperature perturbation field, which are mth order Bessel functions $J_m(kr)$, we can estimate the width of the convection structure in radial direction to be $\delta r \approx X_m/k$, where $X_m \approx 3$ is the width of an oscillation period for Bessel functions, and k has to satisfy a dispersion relation[10]. Since k increases with Ω, the radial width of the wall states decreases as Ω increases. We can reasonably argue that the wavelength at the middle of this width is $O(d)$, independent of rotation. Then $m_c(\Omega) = 2\pi(r - \delta r/2)/\lambda \approx 2\pi(\Gamma - X_m/kd)$, which gives for Γ=2.5 an asymptotic critical mode of $\mathrm{m}_c \approx 16$. This explains why the critical mode number increases with Ω but saturates at about $2\pi\Gamma$.

In addition to the quantitative measurements presented above we performed a series of qualitative investigations to test the relevance of different cell geometries and side wall boundary conditions. In one arrangement a circular plexiglass wall of half the radius of the convection cell was place concentrically inside the cell, thus forming an annulus of width to depth ratio 1.2. Upon increasing R above R_{cs}, wall states formed on all sides of the walls. In the annulus there was a traveling wave (TW) on the outer rim that traveled opposite to the direction of rotation while on the inner rim the TW traveled in the same direction as the rotation direction. In another arrangement, horizontally straight plexiglass walls were placed inside the cell, one side of which was covered with a thin copper tape providing an effectively conducting side wall boundary condition. TWs formed on the insulating side wall at R_{cs} but were suppressed on the conducting wall. The direction of the TWs is $\vec{\Omega} \times \vec{n}$ where $\vec{\Omega}$ is the rotation vector and $\vec{n}$ the the normal vector

Figure 4: Marginal stability boundary in parameter space of R and azimuthal wavenumber k (•) and $\omega_{\kappa 0}$ vs k (□) for $\Omega = 544$ with $\Gamma = 2.5$. The solid line is a nonlinear third-order polynomial fit to the marginal stability data, the short-dashed line is the finite-size Eckhaus boundary, and the long-dashed line is a linear fit to the frequencies.

of the wall into the fluid. A straight wall can thus be considered as the side wall for an effectively infinite convection cell. Kuo and Cross have recently calculated the properties of this straight wall state using free-free top and bottom boundary conditions and rigid boundary conditions at the lateral wall.[12]

The amplitude of the wall convection state is concentrated near the side wall and behaves rather like a quasi-one-dimensional periodic pattern along the circumference. At $\Omega = 544$, we prepared several states with different mode numbers by jumping to a high ΔT and quickly dropping back to just above the critical ΔT. We then measured the amplitude of the traveling wall state and determined the marginal stability boundary by extrapolating the squared amplitude versus R to zero. Figure 4 shows this marginal stability boundary and the corresponding precession frequency measured for $\Omega = 544$ in the $\Gamma = 2.5$ cell. From fits to the data we obtain $R_c = 44217$, $k_c = 4.65$, and $\omega_{\kappa 0c} = 28.3$. The actual switching of mode number toward the critical one

Figure 5: Temperature amplitude squared A^2 ($\bullet$) and frequency $\omega_\kappa 0$ ($\triangle$) vs R for the transition from mode 13 to mode 12.

occurred at finite amplitudes, suggesting an instability other than marginal instability. To identify this instability, we prepared an $m = 13$ state at $R = 4.63\ times10^4$ and ramped down to $R_{cs}(m = 12)$ over about 80 hours making measurements at intervals of $\delta R \approx 0.002$. We define ϵ in terms of $R_c = 44217$ for the marginal stability curve. At $R = 4.547 \times 10^4$, $\epsilon = 0.0283$ with $R_c = 44217$ for the marginal curve, traveling wave's amplitude began to deviate from a linear dependence on R (see Figure 5). The transition to the critical mode number $m_c = 12$ took place 27 hours ($32\tau_\kappa$) later. The extrapolated marginal stability of the $m = 13$ mode is at $R = 4.469 \times 10^4$ ($\epsilon = 0.0107$). Fig. 5 also shows the measured precession frequencies scaled by τ_κ.

Because of the quasi one-dimensionality of the traveling wall states, it should be described by a 1-D complex Ginzburg-Landau (CGL) equation,

$$\tau_0 \left(\frac{\partial A}{\partial t} + s_0 \frac{\partial A}{\partial x} \right) = \epsilon(1 + ic_0)A + \xi_0^2(1 + ic_1)\frac{\partial^2 A}{\partial x^2} - g_0(1 + ic_3)|A|^2 A.$$

Since the precession is opposite to the rotation direction frequencies are negative. We have measured all the coefficients in the CGL equation at $\Omega = 544$,

and they are $c_0 = 0.6,\ c_1 = 0.6,\ -0.01 < c_3 < 0,\ \tau_0 = 0.027,\ s_0 = 2.1,\ \xi_0 = 0.192$, and $g_0 = 0.8$, scaling time by d^2/κ and length by d. In this equation, ϵ is defined relative to $R_c = 44217$ and the modulation wavenumber relative to k_c =4.65, both obtained from the fit to the marginal stability curve, Fig. 4. Using these definitions we obtain the linear coefficients as follows: ξ_0 is the quadratic curvature of the marginal stability curve, Fig. 4 ; τ_0 is obtained from transient measurements of the oscillation amplitude; s_0 is the slope of the frequency at the critical wavenumber, Fig. 5; the combination $c_1 - c_0$ is determined from the curvature of the frequency dispersion, Fig. 5; the combination $c_3 - c_0$ comes from the variation of frequency with ϵ. To resolve the remaining degree of freedom we measure the transient frequency response. To double check our result that c_3 is small we use a modulation technique in which we sinusoidally vary the bottom plate temperature with a period larger than $5.2\tau_\kappa$. This method allows us to probe several parameters at once and to develop better statistics than is possible for the single transient measurements. These results are consistent with the values obtained through the other static and dynamic measurements. The nonlinear coefficient is obtained by normalizing the local probe temperature with the heat transport using $Nu - 1 = |A|^2 R/R_c$ and with an area correction since the traveling-wave state is confined to a region near the wall of order the depth of the fluid (we take a radial width d so $g_0 = (dNu/d\epsilon)(\Gamma^2/(2\Gamma - 1))$. We can compare our linear coefficients, c_0, c_1, τ_0, s_0, and ξ_0 with predictions of the linear theory for our particular experimental conditions[17] which yield $c_0 = 0.7,\ c_1 = 0.8,\ \tau_0 = 0.022,\ s_0 = 1.8$, and $\xi_0 = 0.21$, in reasonable agreement with the experimental values. As in the experiments the CGL equation is not exact so there are finite size uncertanties in the numerical coefficients. Infinite-system, nonlinear calculations [12] for a traveling-wave convection state on a flat wall for Ω=540 and with free-free top-bottom boundary conditions yield $c_0 = 0.8,\ c_1 = 0.45,\ c_3 = 0.32,\ \tau_0 = 0.022,\ s_0 = 2.1, \xi_0 = 0.22$, and $g_0 = 0.6$. Here again the agreement between theory and experiment is quite satisfactory except with regard to the nonlinear coefficient c_3. For more quantitative comparisons the calculations need to incorporate rigid-rigid boundaries and the experimental geometry needs to be changed to accomodate many more periods, thereby better approximating the large-system limit. From the experimental values one obtains $1 + c_1 c_3 > 0$ (the Newell criterion) indicating that the uniform traveling wave pattern is Benjamin-Feir stable. The stability of the traveling wave is bounded by the Eckhaus stable

wavenumber band[15]

$$\epsilon_E = \frac{2(1+c_3^2)+1+c_1c_3}{1+c_1c_3}\xi_0^2(k-k_c)^2.$$

Outside this stability boundary, the pattern is unstable to long wavelength perturbations and will undergo a subcritical bifurcation to a new pattern with a wavenumber within the stability boundary. Given the experimentally obtained values for c_1 and c_3, we find that $\epsilon_E = 3\xi_0^2(k-k_c)^2 = 3\epsilon_M$. In Fig. 4, we plot this Eckhaus boundary with finite size corrections[16]. This boundary agrees well with the experimental evidence that a transition took place around $\epsilon = 0.0283$ when $\epsilon_M = 0.0107$. Since the transition was from $m = 13$ to $m = 12$, both the amplitude and the precession frequency contained progressively more $m = 12$ component, thus becoming larger than if the state was purely mode 13, see Fig. 5. We observed this variation during the transition. Since our cell is very uniform and the quasi one dimensional wall convection structure is strictly periodic, there is virtually no long wavelength perturbation to force the instability to occur. This gives rise to long-lived "metastable" states (Zhong *et al*) when certain wall states have non-critical mode numbers that are outside the Eckhaus stability boundary.

3.2 Bulk convection state

As ΔT increased above the first bifurcation to the wall state, we observed a second transition in the Nusselt number measurements. Accompanied with this rise in heat transport, we also observed convective motion throughout the cell (the "bulk" state) and an increase in the thermal noise in the bottom plate which was supplied with a constant heat power. This indicates that the second transition was to time dependent convection, which was confirmed by analyzing time sequences of many shadowgraph images of the convection pattern.

To characterize the bulk convection state, we measured its critical Rayleigh number R_{cb} and critical wavenumber k_{cb} for $\Omega < 2145$. The critical Rayleigh numbers, determined from heat transport measurements, are shown in Figure 1. Also plotted as a solid line is Chandrasekhar's linear stability analysis result for a laterally infinite system[1]. The critical wavenumbers obtained from recorded shadowgraph images are shown in Figure 6. They also agree well with the results of Chandrasekhar, shown as the solid line. From each

Figure 6: The critical bulk wavenumber k_{cb} vs Ω for the bulk state obtained from shadowgraph images. The solid line is from Chandrasekhar[1].

shadowgraph image, we extracted their central portions, applied 2-D Fourier transformation with band pass frequency filtering and summed up the total power. Just above the onset where the shadowgraph image intensity variation is almost linear in the temperature gradient, the total power in the spectrum is $\sum_i |A_i|^2$ if the convection structures are composed of rolls of $A_i exp(i\vec{k}_i \cdot \vec{x})$. In Figure 7 (a), (b) and (c), we show the background-divided and digitally-enhanced images of the convection patterns with $\Omega = 2145$ for values of R just below, nearly at and slightly above R_{cb}, which was determined from the change in slope of the Nusselt number. The ϵ values in the figure are defined relative to R_{cb}. To more easily compare the bulk amplitude obtained from spectral analysis and heat transport data, we define an effective Nusselt number as the ratio of heat conducted by both convection states (bulk and side-wall) divided by the heat conducted by the side-wall state alone. Figure 7 (d) shows this effective Nusselt number and $\sum_i |A_i|^2$ versus ϵ for $\Omega = 2145$. The linear relation between the total squared amplitude and ϵ confirms that the bifurcation is forward. We conclude that the bulk convection state is the one given by Chandrasekhar's linear stability analysis[1]; because there is no appreciable amplitude of the side-wall state in the central portion the bulk

Figure 7: Shadowgraph images of convection pattern (a) below ($R = 4.87 \times 10^5$, ϵ = -0.062), (b) nearly at (R = 5.11 $times 10^5$, ϵ = -0.016), and (c) above ($R = 5.38 \times 10^5$, $\epsilon = 0.037$) the onset of bulk convection, and (d) the effective Nusselt number Q/Q́ (•), ie. the ratio of the total heat conducted in the convecting state divided by the heat conducted by the side-wall state alone, and the squared amplitude (□) vs ϵ. All the data are for $\Omega = 2145$ and the ϵ values for the patterns are labeled in (d).

state can grow from small amplitude despite being a second transition.

Figure 1 shows that the bifurcation lines for the side wall state and the bulk convection state cross each other when $60 < \Omega < 70$ for $\Gamma = 2.5$. For Ω less than the intercept value, bulk convection sets in first and wall convection begins later. The bulk and wall convections are spatially separated, interacting only weakly. The cross-over point for the bifurcation lines is therefore not a co-dimension two point. A further point about this regime at small Ω is that the small aspect ratio of the container may become important. Qualitatively nothing changes but for the quantitative comparison with theory these finite size effects are probably significant. In particular, the bulk state is the initial bifurcation and its presence might strongly influence the side-wall bifurcation which now happens at higher R; the high value, relative to theory, of the side-wall onset for $\Omega = 16.93$ suggests such an effect. The onset of the bulk state is also affected by the small aspect ratio when Ω is small as evidenced by the small upward shift of R_{cb} consistent with finite-size effects in non-rotating convection[19, 20]. Both of these shifts are visible in Fig. 1.

There are several additional interesting aspects of the results obtained from shadowgraph images. First, there is a range of R around R_{cb} where the convection pattern in the middle region consists of concentric rings. As is known[18], concentric ring patterns in Rayleigh-Bénard convection can be induced by thermal forcing from the side wall owing to the mismatch of thermal conductivities between the side wall and working fluid. In our case, the effective side wall for the bulk convection is the wall state, which is convecting rather vigorously at the second bifurcation point. For $\Omega = 1090$ and near the onset of bulk convection ($R/R_{cs} = 2.246$), $Nu = 1.54$. The active convection area is at most 50% of the cell, implying an effective thermal conductivity of the wall state at least twice that of the conducting water in the middle. The concentric rings eventually break up when ϵ is increased and give rise to cellular structures.

The total squared amplitude ($\sum_i |A_i|^2$), shown in Figure 7 (d), has a linear dependence on R. However, the extrapolation of this linearity to the base line yields a Rayleigh number slightly less than R_{cb}, typically on the order of 0.2%. Judging from the rounded corner of the Nu versus ϵ curve near $\epsilon = \epsilon_2$, this shift is caused by the appearance of the concentric ring pattern.

A time sequence of the images taken at different points in parameter space reveals the source of the time dependence in the bulk convection state. For

Ω as high as 2145, we observed a Küppers-Lortz roll-orientation switching and/or turbine like rotation of convection cells. The dynamics stemming from the Küppers-Lortz instability are aperiodic, which gives rise to the increased thermal noise in the bottom plate. This aspect of the result will be presented in greater detail elsewhere[21].

4 Conclusion

In this paper, we presented experimental results for the initial bifurcations in rotating Rayleigh-Bénard convection in small aspect ratio cylindrical cells. We confirmed a forward bifurcation from conduction to convection near rigid walls. Our experimental data agree beautifully with the theoretical results for the rotation dependence of the critical traveling wave frequency and mode number. We confirmed the prediction that the critical frequency goes linearly to zero as Ω approaches zero. We also conjecture from the experiment that for insulating walls, the critical mode number will reach an asymptotic finite value as Ω increases. We have shown for the second bifurcation that the convection states are very similar to the ones that are linearly unstable in the infinite system. Because of their spatial separation, the wall and bulk convection states interact only weakly in a narrow annular region between the two states. As aspect ratio increases, the separation becomes more distinct and the wall state becomes relatively more confined to the side wall. Since the wall state is quasi one dimensional, its contribution to the dynamics and transport properties of rotating thermal convection should diminish in the limit of large aspect ratio. The presence of such "surface" modes will, however, subtly affect aspects of the bulk nonlinear dynamics, as is evident by its forcing of the concentric ring pattern near the onset of bulk convection.

The authors wish to thank H. F. Goldstein, E. Knobloch, I. Mercader and M. Net and E. Kuo and M. Cross for allowing us to use their theoretical results prior to publication. We gratefully acknowledge conversations with M. Cross, L. Kramer, W. van Saarloos, L. Tuckerman, and K. Babcock. One of us (RE) would like to acknowledge the Institute for Theoretical Physics at UC Santa Barbara for participation in the program "Spatially-Extended Nonequilibrium Systems." This research was supported by the U.S. Department of Energy.

References

[1] S. Chandrasekhar, Hydrodynamic and Hydromagnetic Stability, Oxford University Press (1961).

[2] R. M. Clever and F. H. Busse, J. Fluid Mech. **94**, 609(1979).

[3] H.T. Rossby, J. Fluid Mech. **36**, 309 (1969).

[4] Fang Zhong, R. E. Ecke and V. Steinberg, Phys. Rev. Lett. **67**, 2473 (1991) and J. Fluid Mech., to be published.

[5] G.H. Homsy and J.L. Hudson, Appl. Sci. Res. **26**, 53 (1972)

[6] J.C. Buell and I. Catton, Phys. Fluids **26**, 892 (1983).

[7] G. Küppers and D. Lortz, J. Fluid Mech. **35**, 609 (1969).

[8] F. H. Busse, Transition and Turbulence, Academic Press (1981).

[9] J. Niemela and R. J. Donnelly, Phys. Rev. Lett. **57**, 2524 (1981).

[10] H. F. Goldstein, E. Knobloch, I. Mercader and M. Net, preprint (1992).

[11] R. E. Ecke, F. Zhong, and E. Knobloch, Europhys. Lett. **19** (3), 177 (1992).

[12] E. Kuo and M. Cross, private communication.

[13] P. Manneville, Dissipative Structures and Weak Turbulence, Academic Press (1990).

[14] G. Veronis, J. Fluid Mech. **5**, 401 (1959).

[15] B. Janiaud, A. Pumir, D. Bensimon, V. Croquette, H. Richter, and L. Kramer, Physica **55D**, 269 (1992)

[16] L. Tuckerman and D. Barkely, Physica **D46**, 57 (1990).

[17] I. Mercader, M. Net, and E. Knobloch, private communication.

[18] G. Ahlers, M. C. Cross, P. C. Hohenberg, and S. Safran, J. Fluid Mech. **110**, 297 (1981).

[19] G. Charlson and R. Sani, Int. J. Heat Mass Transfer, **13**, 1479 (1970).

[20] K. Stork and M. Müller, J. Fluid Mech. **71**, 231 (1975).

[21] Li Ning and R. E. Ecke, unpublished.

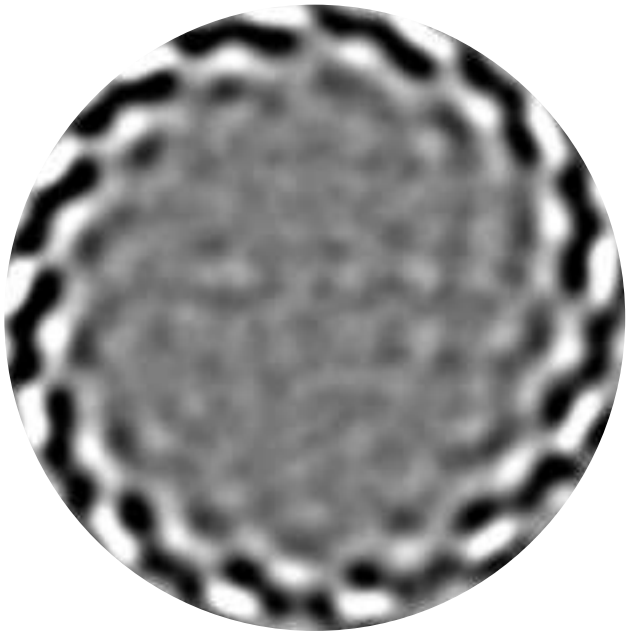

(a)

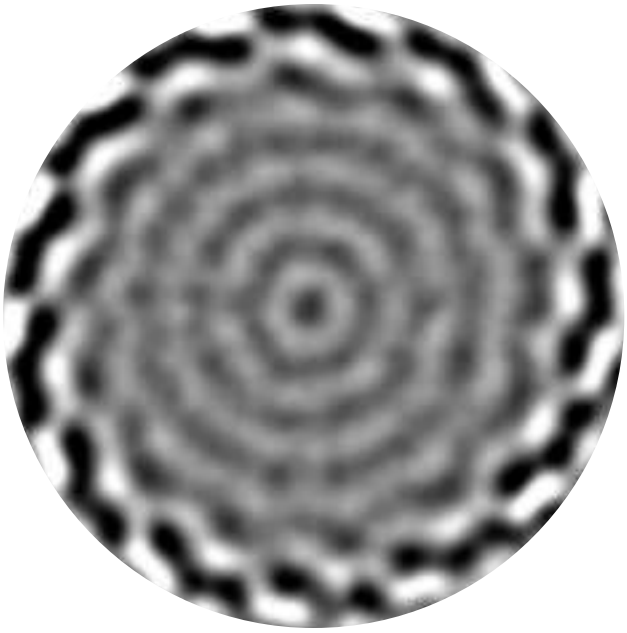

(b)

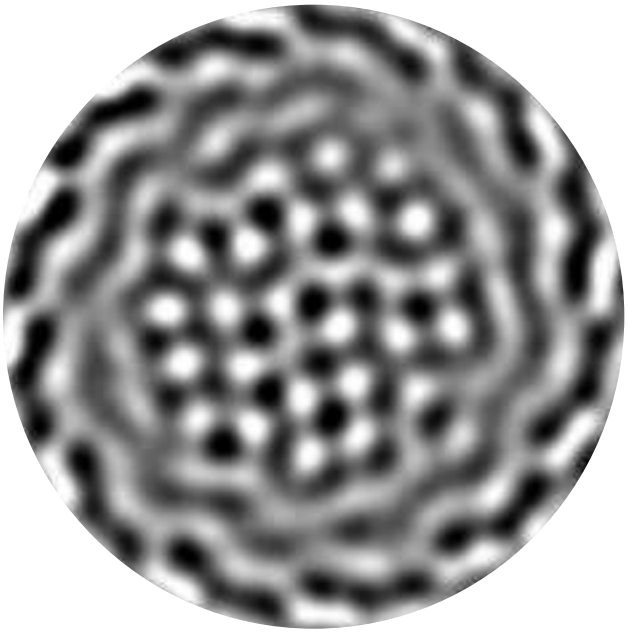

(c)

(d)